Climate
of the Past

Warming drove the expansion of marine anoxia in the equatorial Atlantic during the Cenomanian leading up to Oceanic Anoxic Event 2

Mohd Al Farid Abraham[1,2], **Bernhard David A. Naafs**[1], **Vittoria Lauretano**[1], **Fotis Sgouridis**[3], **and Richard D. Pancost**[1]

[1]Organic Geochemistry Unit, School of Chemistry and School of Earth Sciences,
University of Bristol, BS8 1TS, United Kingdom
[2]Geology Programme, Faculty of Science and Natural Resources, Universiti Malaysia Sabah,
Jalan UMS, 88400, Kota Kinabalu, Sabah, Malaysia
[3]School of Geographical Sciences, University of Bristol, BS8 1SS, United Kingdom

Correspondence: Mohd Al Farid Abraham (al.farid@ums.edu.my)

Abstract. Oceanic Anoxic Event 2 (OAE 2) ($\sim$ 93.5 Ma) is characterized by widespread marine anoxia and elevated burial rates of organic matter. However, the factors that led to this widespread marine deoxygenation and the possible link with climatic change remain debated. Here, we report long-term biomarker records of water-column anoxia, water-column and photic zone euxinia (PZE), and sea surface temperature (SST) from Demerara Rise in the equatorial Atlantic that span 3.8 Myr of the late Cenomanian to Turonian, including OAE 2. We find that total organic carbon (TOC) content is high but variable (0.41 wt %–17 wt %) across the Cenomanian and increases with time. This long-term TOC increase coincides with a TEX$_{86}$-derived SST increase from $\sim$ 35 to 40 °C as well as the episodic occurrence of 28,30-dinorhopane (DNH) and lycopane, indicating warming and expansion of the oxygen minimum zone (OMZ) predating OAE 2. Water-column euxinia persisted through much of the late Cenomanian, as indicated by the presence of C$_{35}$ hopanoid thiophene but only reached the photic zone during OAE 2, as indicated by the presence of isorenieratane. Using these biomarker records, we suggest that water-column anoxia and euxinia in the equatorial Atlantic preceded OAE 2 and this deoxygenation was driven by global warming.

1 Introduction

Ocean Anoxic Event (OAE) 2, which occurred at the Cenomanian–Turonian boundary (CTB, 93.5 Ma), is the last major Cretaceous anoxic event (Jenkyns, 2010) and lasted around 430 to 700 kyr (Voigt et al., 2008; Meyers et al., 2012; Eldrett et al., 2015). It is characterized by a global decline in ocean oxygenation and widespread burial of black shales rich in organic matter (OM) (Schlanger and Jenkyns, 1976; Jenkyns, 2010). Additional evidence for the enhanced burial of ^{13}C-depleted OM comes from the globally recorded positive stable carbon isotope (δ^{13}C) excursion across OAE 2 (Schlanger et al., 1987; Erbacher et al., 2005; Jarvis et al., 2006; Sinninghe Damsté et al., 2010; Takashima et al., 2010; Jarvis et al., 2011). Notably, carbon burial rates and the magnitude of the positive carbon isotope excursion (CIE) vary among regions, with southern North Atlantic sites, for example, characterized by particularly high organic matter content, with total organic carbon (TOC) content of 50 % (Monteiro et al., 2012, and references therein) and CIEs up to 6 ‰ (Arthur et al., 1988; Erbacher et al., 2005).

For more than 40 years (Schlanger and Jenkyns, 1976), the causal mechanisms for OAE 2 have remained contested, but the leading hypothesis is that a large input of volcanically sourced carbon dioxide into the atmosphere (Barclay et al., 2010), associated with the emplacement of the Caribbean Large Igneous Province (CLIP; Snow et al., 2005) and the

High Arctic Large Igneous Province (HALIP; Schröder-Adams et al., 2019), increased global temperatures. Subsequent feedback mechanisms, such as an increase in continental weathering (Pogge Von Strandmann et al., 2013), led to an enhanced ocean nutrient budget that fuelled high productivity regimes that were further supported by ocean upwelling (Lüning et al., 2004). These phenomena drove widespread marine deoxygenation and led to higher organic carbon (OC) burial rates around the world (Jenkyns, 2010; Monteiro et al., 2012). Potentially, as much as 50 % of the ocean volume was deoxygenated during OAE 2 based on model experiments (Monteiro et al., 2012), although other approaches yield lower estimates (Clarkson et al., 2018). Regardless, there is strong evidence for widespread marine deoxygenation, which impacted key biogeochemical cycles (Naafs et al., 2019).

However, these mechanisms are dependent to various degrees on pre-conditioning and the background state of the mid-Cretaceous ocean and climate. A compilation of sea surface temperature (SST) across the Cretaceous shows that the Cenomanian was characterized by the highest values of the Cretaceous, with tropical sites reaching temperatures over 35 °C (O'Brien et al., 2017), but the detailed evolution of SSTs remains poorly constrained. Changes in organic burial rates in the proto-North Atlantic Ocean, both during OAE 2 and preceding it, could have been caused by these high temperatures; alternatively, they could highlight the role of marine gateways in controlling the incursion of oxic or anoxic water masses that induced widespread marine anoxia (Laugié et al., 2021). Scaife et al. (2017) suggested that the mid-Cenomanian Event (MCE; 96.49; Batenburg et al., 2016) was a prelude to the onset of the OAE 2, characterized by mercury evidence for subaerial LIP emplacement and a positive CIE of $\sim 1\%o$ (Jarvis et al., 2006; Joo and Sageman, 2014; Joo et al., 2020).

Here, we explore the detailed Cenomanian evolution of marine anoxia and its link with SSTs at Ocean Drilling Programme (ODP) Leg 207 Demerara Rise in the equatorial North Atlantic Ocean. ODP Leg 207 comprises five sites (1257 to 1261) that recovered sediments ranging from the Albian to the Pleistocene (Erbacher et al., 2004). Notably, the occurrence of marine anoxia and photic zone euxinia in this basin has been previously reported from proximal site 1260 using the biomarker lycopane and trace metals that increase in abundance before and during OAE 2 (van Bentum et al., 2009). However, that study only reported the latest part of the Cenomanian prior to OAE 2.

The sediment from the more distal and deeper site 1258 could provide an extended Cenomanian succession and a long-term palaeo-environmental record of the late Cenomanian. We determined the occurrence of water-column anoxia using the biomarker 28,30-dinorhopane (Moldowan et al., 1984). Water-column anoxia was also reconstructed using lycopane as a proxy for the oxygen minimum zone (OMZ; Sinninghe Damsté et al., 2003; Adam et al., 2006), com-

plementing the published record from site 1260 (van Bentum et al., 2009). Additionally, we reconstruct water-column euxinia (sulfidic condition) based on the occurrence of C_{35} hopanoid thiophenes (Valisolalao et al., 1984; Sinninghe Damsté et al., 1995). The expansion of euxinic conditions into the photic zone was reconstructed based on the abundance of the biomarker isorenieratane (Sinninghe Damsté et al., 2001), extending the record from site 1260 (van Bentum et al., 2009). In parallel, we reconstructed SST at site 1258 based on the membrane lipids (isoGDGTs) of Thaumarchaeota – TEX_{86} (TetraEther indeX of 86 carbons; Schouten et al., 2002; Kim et al., 2010) – expanding on the previously published low-resolution data from site 1258 (Forster et al., 2007). Ultimately, we link this high-resolution record of water-column anoxia and euxinia with the evolution of climate (e.g. SST) during the Cenomanian and test the hypothesis that warming drove ocean deoxygenation during the 3.7 Myr preceding OAE 2.

2 Site location

Ocean Drilling Programme (ODP) Leg 207 site 1258 of Demerara Rise is a deep-water site at 3192.2 m below sea level on the continental shelf north of Suriname in the equatorial Atlantic. During the Cenomanian this site was located at a latitude of $\sim 5°$ N (Fig. 1). This study investigated 123 sediments from site 1258 (hole B) cored to 460.9 m below sea floor, with a sample recovery of 76.3 % and spanning the Cenomanian to Turonian. The lithostratigraphic units of the interval were defined as black finely laminated calcareous claystone with relatively high organic matter content (Unit IV). It is stratigraphically underlain by Albian phosphoritic calcareous claystone (Unit V). Meanwhile, during the Campanian to Miocene the sediments mainly comprise calcareous and siliceous microfossils and clay (Units III to I). Total organic carbon content at site 1258 increases from the Albian to the Cenomanian–Turonian boundary (CTB) with a maximum of ~ 28 wt % over the OAE 2 interval; much lower TOC content are found following the CTB. Carbonate content ranges from 30 % to 80 %, with lowest values (~ 5 %) occurring in OAE 2 interval. The OAE 2 interval itself is identified at site 1258 based on a positive excursion in $\delta^{13}C_{org}$ values by $\sim 6\%o$, consistent with previous studies and global change in the C cycle (Sageman et al., 2006; Li et al., 2017). Limited carbonate preservation has hindered the effort to constrain $\delta^{13}C_{carb}$ across OAE 2.

Due to extensive prior sampling, relatively few sediments remain from the OAE 2 interval, and here we predominantly focus on the long-term trends during the Cenomanian leading up to this event. The age–depth model for the Cenomanian are based on published data (Friedrich et al., 2008) and three tie points: (a) the Middle Cenomanian event (95.7 Ma), (b) the last occurrence of the nannofossil marker *Corollithion kennedyi* (94.1 Ma), and (c) the onset of the OAE 2 posi-
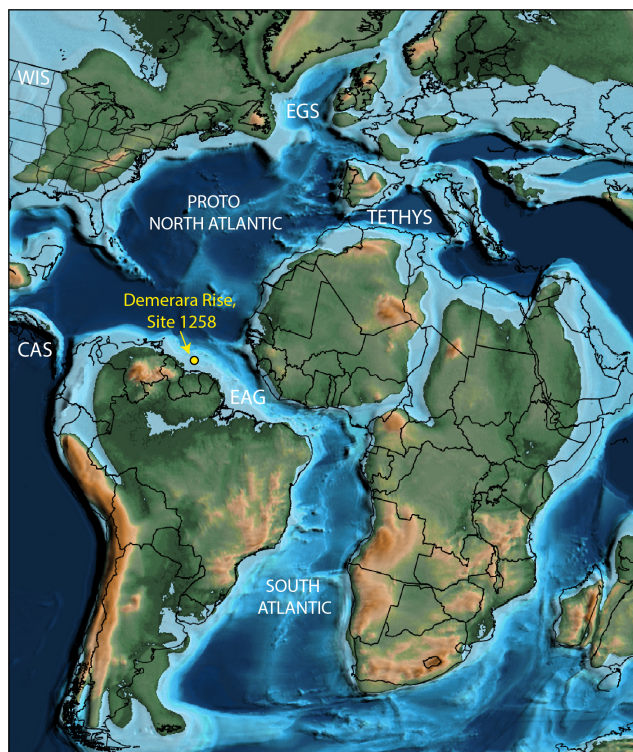
Figure 1. Palaeo-geographic location of ODP site 1258, Demerara Rise (modern latitude: 9°27.23′ N; 54°20.52′ W, yellow circle), during the Cenomanian (~ 95 Ma). The map is from Scotese (2021) and shows land (green), continental shelves (light blue), deep water (dark blue), and modern territorial boundaries (solid black lines). Also shown are five potentially important marine gateways; the Equatorial Atlantic Gateway (EAG), Central America Seaway (CAS), Western Interior Seaway (WIS), East Greenland Gateway (EGS), and Tethys Seaway.

tive carbon excursion (~ 300 kyr prior to CTB; 93.8 Ma; Erbacher et al., 2005). The interval of OAE 2 at site 1258 (422 to 426 m composite depth) is estimated to have lasted for 550 kyr (Meyers et al., 2012).

3 Materials and methods

The stable carbon isotopic composition of bulk organic matter ($\delta^{13}C_{org}$; expressed relative to Vienna PeeDee Belemnite) and total organic carbon (TOC; wt %) content at site 1258 were analysed on aliquots (5–10 mg) of homogenized black shale samples using an elemental analyser (EA) coupled with an Elementar isoprime precisION isotope-ratio mass spectrometer (IRMS), following carbonate removal from the samples via acidification as described by Hedges and Stern (1984). Analyses were carried out in duplicates with the average reported here (standard deviation < 0.3). The instrument was normalized using organic reference materials of USGS61 ($-35.05 \pm 0.04‰$), USGS62 ($-14.79 \pm 0.04‰$), and USGS63 ($-1.17 \pm 0.04‰$), as reported by Schimmel-

mann et al. (2016). These new $\delta^{13}C$ and TOC data were combined with published data from site 1258 (Erbacher et al., 2005; Friedrich et al., 2008).

For biomarker characterization, we extracted 5 g each of 123 ground samples with 15 mL of a dichloromethane : methanol (DCM : MeOH; 9 : 1, v/v) azeotrope using an ETHOX EX microwave extraction system. Prior to extraction, 2500 ng of 5α-Androstane were added as an internal standard. The total lipid extract (TLE) was separated via column chromatography into apolar and polar fractions with 4 mL of hexane : DCM (9 : 1, v/v) and 3 mL of DCM : MeOH (1 : 2, v/v) respectively. The apolar fraction, containing the anoxia and euxinia biomarkers, was analysed using a Thermo Scientific™ ISQ Series Single Quadruple gas chromatography–mass spectrometer (GC-MS). The separation of compounds was performed on a Zebron non-polar column (50 m $\times$ 0.32 mm, 0.10 μm film thickness). The injection volume was 1 μL, and the GC was programmed for injection at 70 °C (1 min hold), heating to 130 °C at a rate of 20 °C min^{-1}, then to 300 °C at 4 °C min^{-1}, followed by a 24 min hold. The carrier gas was helium, with a flow rate of 3 mL min^{-1}. The GC-MS continually scanned over m/z 50 to 650. It was operated in election ionization (IE) mode at 70 eV at ion source temperature of 200 °C, and the interface temperature between GC and MS was maintained at 300 °C. To monitor instrument stability, a fatty acid methyl ester standard mixture was injected daily.

The concentration of biomarkers was determined by integrating the peak on a partial mass chromatogram (m/z) of known fragments ion of biomarkers relative to the peak area of the standard on the same m/z trace. Due to the variety of response factors, we do not convert these to true concentrations. The biomarkers were identified based on published spectra, characteristic mass fragments and retention times. Briefly, the C_{28} 28,30-dinorhopane (DNH) that serves as a proxy for water-column anoxia was identified based on m/z 191, 163, and 384 fragments (Moldowan et al., 1984). Lycopane, which indicates the presence of an oxygen minimum zone, was identified based on m/z 71, 113, 183, 253, 309, 337, 407, and 477; $M+ = 563$, but it co-elutes with the $C_{35}n$-alkane (Sinninghe Damsté et al., 2003). The incorporation of sulfur into biomarkers indicates water-column euxinia and is traced using the C_{35} hopanoid thiophene, identified from its m/z 191, 369, and 97 (Valisolalao et al., 1984). Photic zone euxinia (PZE) was reconstructed based on the biomarker isorenieratane, C_{40} compounds with characteristic fragments of m/z 133, 134 and $M+ = 546$ (Koopmans et al., 1996).

The polar fractions containing the glycerol dialkyl glycerol tetraethers (GDGTs) were dissolved in hexane : isopropanol (99 : 1, v/v) and passed through 0.45 μm polytetrafluoroethylene filters prior to single ion monitoring (SIM) analysis on a ThermoFisher Scientific Accela Quantum Access triple quadrupole mass spectrometer coupled to a high-performance liquid chromatography–mass spectrom-

etry (HPLC-MS) system. The LC instrument methods followed Hopmans et al. (2016). To reconstruct TEX_{86}-based SST (Schouten et al., 2002), we evaluated secondary influences on TEX_{86} using established GDGT indices such as the branched and isoprenoid tetraether index (BIT index) to preclude excessive soil input (Hopmans et al., 2004); percentage of GDGT-0 (Sinninghe Damsté et al., 2012) to evaluate potential contributions from methanogenic archaea, the methane index (Zhang et al., 2011) to preclude contributions from methanotrophic Euryarchaeota, and the GDGT-2 / GDGT-3 ratio that distinguishes the contribution of deep-marine (high ratio) versus shallow subsurface (low ratio) ammonia-oxidizing Thaumarchaeota (Taylor et al., 2013). Then, TEX_{86}-based SSTs were determined using the "deep-time" approach of the Bayesian, spatially varying regression (BAYSPAR) model with a prior of $30 \pm 20 °C$ and search tolerance of 3 standard deviations, using MATLAB (Tierney and Tingley, 2014). We combined our higher-resolution data with previously published TEX_{86} records from site 1258 (Forster et al., 2007), converting them to SST using the same BAYSPAR methodology.

4   Results

The long-term $\delta^{13}C_{org}$ record, based on a combination of data from this study and published data (Erbacher et al., 2005; Friedrich et al., 2008), is relatively stable throughout most of the Cenomanian, 97 to 93.8 Ma (467 to 426 m), ranging from -30 to $-27 ‰$ and increasing slightly through the Cenomanian (Fig. 3a). A major positive excursion up to maximum values of $\sim -21 ‰$ marks the OAE 2 interval between 93.8 to 93.5 Ma (422 to 426 m). TOC content varies dramatically but gradually increases from 1 wt % to 17 wt % in pre-OAE Cenomanian sediments and reaches the highest values of 28 wt % in the OAE 2 interval (Fig. 3b).

TEX_{86}-based SSTs, based on the BAYSPAR calibration of Tierney and Tingley (2014), decrease slightly during the early Cenomanian from an average of $\sim 34 °C$ to a minimum of $\sim 32 °C$ (95.73 Ma) in the mid-Cenomanian, coinciding with the Mid-Cenomanian positive carbon isotope Excursion (MCE; Fig. 3c). The SST then exhibits a significant long-term – but episodic – increase, reaching a maximum of $\sim 43 °C$ at around 93 Ma. Our reported SSTs are about 2.6 °C lower than those of Forster et al. (2007), likely due to interlaboratory variations in LC-MS conditions and modified LC-MS analytical protocol (Schouten et al., 2013). There is no evidence for secondary influences on isoprenoidal GDGT distributions that would preclude their use in SST estimation. The Cenomanian average for the BIT Index is 0.1 (Hopmans et al., 2004; Weijers et al., 2006) and the Methane Index is 0.2 (Zhang et al., 2011), both of which are low (Table S2 in the Supplement). GDGT-2/GDGT-3 ratios have been used to explore the balance of shallow vs. deep-dwelling Thaumarchaeota inputs (Taylor et al., 2013). Values here are low
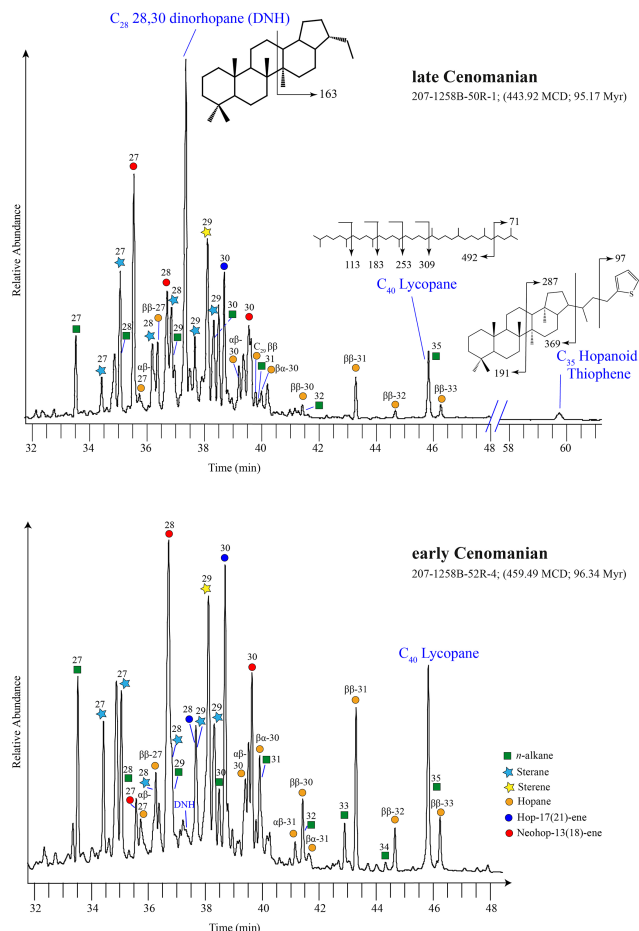

Figure 2. Total ion chromatogram (TIC) of the apolar fraction of two typical Cenomanian samples at 96.34 and 95.17 Ma. The partial mass structures indicate the targeted biomarkers used to determine the water-column anoxia using C_{28} 28,30-dinorhopane ($m/z = 191, 163; M+ = 384$); oxygen minimum zone based on lycopane (m/z 71, 113, 183, 253, 309; $M+ = 492$). The transition from anoxic to euxinic water column is indicated by the presence of C_{35} hopanoid thiophene that is absent during the early Cenomanian. The carbon number indicates from the number above the key symbols that represent suites of n-alkanes, steroids, and hopanoids.

(average 2.2), suggesting that the isoprenoidal GDGTs are predominantly derived from the shallow water ammonia-oxidizing Thaumarchaeota community, and they are consistent with GDGT-2/GDGT-3 values throughout the Mesozoic (average of 2.6) (Rattanasriampaipong et al., 2022). These values are lower than those in modern oceans, and it remains unclear if this affects reconstructed SSTs (Rattanasriampaipong, 2022), but the lack of any long-term change in GDGT-2/GDGT-3 ratios in Cenomanian Demerara Rise sediments indicates that secular trends are robust.

The relative abundance of dinorhopane (DNH; abundance relative to total hopanes; Fig. 3d), a biomarker indicative of water-column anoxia (Peters et al., 2004), is low in the early Cenomanian, exhibits multiple maxima in the mid-
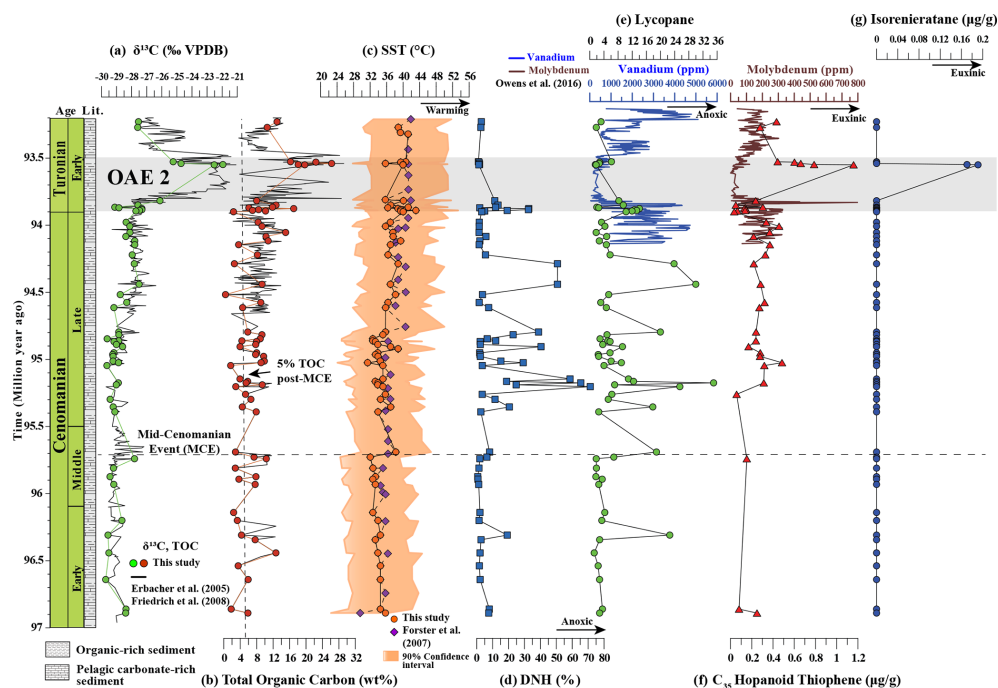
Figure 3. Stable isotopic composition, TOC, and biomarker records for site 1258 at Demerara Rise. From left to right, **(a)** stable carbon isotopic composition of bulk organic matter, combining data from this study and published data (Erbacher et al., 2005; Friedrich et al., 2008), **(b)** total organic carbon (TOC) content (new data and published data (Erbacher et al., 2005; Friedrich et al., 2008)), **(c)** deep-time BAYSPAR-calibrated TEX_{86}-based SST based on data of this study and Forster et al. (2007), **(d)** 28,30-dinorhopane/total $C_{27}–C_{35}$ hopane ratio in percentage, **(e)** (lycopane + $C_{35}n$-alkanes)/$C_{31}n$-alkanes (lycopane) index, **(f)** concentration of C_{35}-hopanoid thiophene, and **(g)** concentration of isorenieratane. The calibration uncertainty for BAYSPAR-calculated TEX_{86}-based SST is $\pm 3.5\,°C$, which is approximate to the mean ($n = 123$) width of 90 % confidence interval. Also shown in blue and brown are vanadium and molybdenum concentrations respectively, showing their dramatic drawdown during OAE 2 (Owens et al., 2016).

dle and late Cenomanian sediments, but is again low during OAE 2. The lycopane index (Fig. 3e), also indicative of water-column anoxia and/or an expanded oxygen minimum zone (Sinninghe Damsté et al., 2003), closely tracks the DNH relative abundance ($r^2 = 0.67$, Fig. 4). The lycopane index is low in the lowermost part of the section, but from the mid-Cenomanian up to the OAE 2 interval it is highly variable with at least eight maxima and values up to 35 (95.17 Ma). Intriguingly, lycopane indices are relatively low during OAE 2, and this is in agreement with the previously published data from proximal site 1260 of Demerara Rise (van Bentum et al., 2009). Low lycopane and DNH indices from OAE 2 could partially reflect their reaction with hydrogen sulfide and incorporation into a S-bound pool of OM (Sinninghe Damsté et al., 2014), and this is discussed below.

The C_{35} hopanoid thiophene concentrations (Sinninghe Damsté et al., 1990) are low or the below detection limit in lower Cenomanian sediments (Fig. 2), suggesting minimal water-column euxinia. However, concentrations increase from the mid-Cenomanian towards OAE 2 (Fig. 3f). Isorenieratane, derived from the green sulfur bacteria carotenoid isorenieratane (French et al., 2015, and references therein)

and therefore a biomarker for PZE (Sinninghe Damsté et al., 2001), occurs in only two samples, both from the OAE 2 interval, although the sampling resolution for OAE 2 was limited. Crucially, isorenieratane could be partially sequestered in the S-bound fraction of organic matter (Sinninghe Damsté and Köster, 1998; Ma et al., 2021). However, van Bentum et al. (2009) investigated the sulfur-bound biomarkers and reported the occurrence of isorenieratane only in the OAE 2 interval onset at Demerara Rise (site 1260) with no signal prior to the event.

5 Discussion

5.1 Marine anoxia expansion during the Cenomanian

The relatively high TOC content during the Cenomanian suggests that these black shales at site 1258 were deposited under the influence of bottom-water oxygen limitation (Burdige, 2007). Stratigraphically higher than the OAE 2 interval, TOC content decreases to values < 1 wt % (Erbacher et al., 2004), remaining low throughout the Upper Cretaceous and Cenozoic, including during other prolonged and transient greenhouse climates (Frieling et al., 2018). This suggests that these anoxic conditions, driven by high organic matter burial
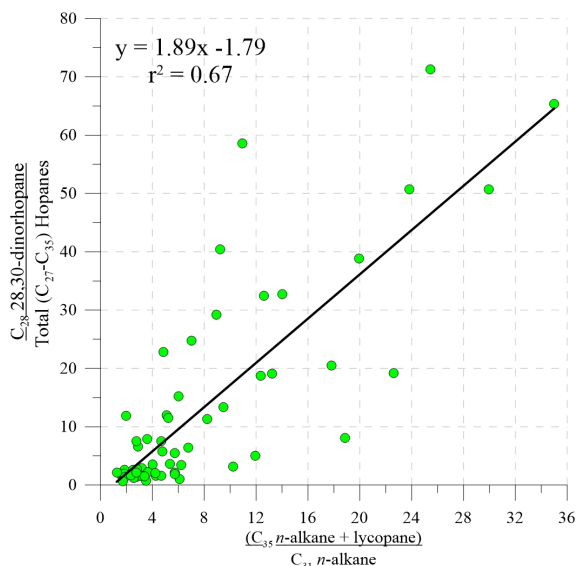
Figure 4. Cross plot of DNH relative abundances and lycopane indices, showing the similar behaviour of these biomarkers, indicative of water-column anoxia throughout the Cenomanian leading up to OAE 2.

rates at Demerara Rise during the mid-Cretaceous, were facilitated by basin geometry during the early opening phases of the South Atlantic (Friedrich and Erbacher, 2006; Donnadieu et al., 2016). However, Cenomanian TOC content also varies on both short and long timescales, the latter most evident in an increase in average TOC content from through the Cenomanian and culminating in the OAE 2 interval (up to 28 wt %), suggesting that basin geometry is not the only factor governing organic matter burial rates.

At the base of the studied interval, TOC content ranges from 1 % to 6 % and indicates that bottom-water suboxic conditions could have been present even during deposition of the lowermost sections from the early Cenomanian (Arthur et al., 1987; Trabucho Alexandre et al., 2010; Berrocoso et al., 2010) and possibly the Albian. TOC content in excess of 5 % becomes common in the mid-Cenomanian, alongside black shale lamination and the absence of benthic bioturbation (Erbacher et al., 2004); these features and the concomitant decrease in the abundances and diversity of foraminifera (Friedrich et al., 2008) indicate bottom water anoxia. Then, in the lead-up to OAE 2, the TOC increases up to 17 wt %, similar to the high TOC of $\sim$ 19 wt % that occurs just below the onset level of OAE 2 at site 367, Cape Verde Basin (Sinninghe Damsté et al., 2008), which is located at the conjugate margin to the east.

As TOC content increases in the mid- to late-Cenomanian, so do the DNH relative abundances and lycopane index. The sediments with elevated DNH proportions are exceptional in the geological record. In our samples, DNH in some cases is the most abundant hopane and even one of the dominant compounds in the apolar fraction; this is rare in rocks of

any age (Słowakiewicz et al., 2015) and has been linked to the persistence of a strong OMZ, such as during the Monterey Event in the Miocene (Sinninghe Damsté et al., 2014). These same DNH-rich horizons have very high lycopane indices, similar to those associated with strong OMZs in today's oceans, including the Black Sea (Sinninghe Damsté et al., 2003). The expansion of anoxia through the water column at Demerara Rise also has been invoked by the low enrichment factor (EF $\sim$ 1) of manganese during most of the Cenomanian (van Bentum et al., 2009), attributed to the dissolution of Mn^{2+} and its mobilization into an expanded OMZ (Hetzel et al., 2006). The decline in benthic foraminifera assemblages from the early to late Cenomanian provides further evidence for oxygen depletion at the sea floor and within the water column (Friedrich et al., 2009). Together, our DNH and lycopane results build on the low-resolution lycopane record of van Bentum et al. (2009) and indicate a long-term increase in water-column anoxia mediated by shorter-term variations.

Intriguingly, both the lycopane and DNH indices are low over the OAE 2 interval. This phenomenon has also been reported for the lycopane index at nearby site 1260 by van Bentum et al. (2009), although their record did not extend far into the Cenomanian. Although there is great spatial variability in OAE 2 conditions (Jenkyns, 2010), the presence of isorenieratane and very high TOC content at sites 1258 and 1260 (van Bentum et al., 2009, and this work) indicate that the most extreme water-column anoxia (and euxinia) at Demerara Rise occurred over the OAE 2 interval. If the lycopane index is driven by its selective preservation relative to terrestrial n-alkanes (Sinninghe Damsté et al., 2003), then we would expect it to also be highest in the OAE 2 interval. Instead, we argue that the low values of both lycopane and DNH indices during OAE 2 were driven by a further expansion of anoxia that favoured other microorganisms at the expense of the lycopane and DNH-producers. In particular, the DNH and lycopane producers, possibly chemoautotrophs living at redox boundaries of a strong OMZ, were replaced over the OAE 2 interval by green sulfur bacteria thriving under euxinic conditions. The co-occurrence of high concentrations of isorenieratane and DNH is uncommon (e.g. Słowakiewicz et al., 2015), suggesting that the respective source organisms require specific and distinct oceanographic conditions. Recent studies suggest that DNH is a diagenetic product of C_{28} 28,30-dinorhopane (Sinninghe Damsté et al., 2014), with both the product and precursor indicating a stratified palaeo-water column. Sulfidic conditions could have contributed to the low measured abundances of lycopane and DNH during OAE 2, as their unsaturated precursors are also prone to sulfurization. However, their abundances do not decrease when water-column euxinia (but not PZE) becomes widespread (see below), and we note that Sinninghe Damsté et al. (2014) argued for rapid diagenetic conversion of C_{28}-dinorhopane (potential precursor) into DNH and aromatic hopanoids that are "shielded" from reactions with sulfide.

Although variations in C_{35}-hopanoid thiophene concentrations do not match those of lycopane indices nor DNH abundances, they do provide evidence for a long-term increase in excess free inorganic sulfide in the water column through the Cenozoic and especially during OAE 2 interval (Fig. 3f). In particular, Sinninghe Damsté et al. (1990) argued that abundant S-bound OM was evidence for water-column euxinia, where OM could compete favourably for reduced sulfur due to the limited availability of reactive iron (Fe). This process also gives rise to the coupling of the S and OC cycles, with sulfurization facilitating OM burial (Werne et al., 2004; Raven et al., 2018) while removing S from the oceans. Intermediate complexity models are consistent with this, showing that rapid sulfurization significantly affects the global ocean during the OAE 2 interval, enhancing organic carbon preservation by over 30 %, speeding up the OAE 2 recovery, and reducing the volume of ocean euxinia by 80 % via H_2S scavenging (Hülse et al., 2019).

Our work adds to inorganic geochemical studies that also argued for a progressive deoxygenation of the southern North Atlantic leading up to OAE 2. For example, a time lag of 75 kyr has been estimated for the dramatic drawdown of ocean vanadium (V; a proxy for water-column anoxia) during the late Cenomanian and that of molybdenum (Mo; a proxy for water-column euxinia) after the onset of OAE 2 (Owens et al., 2016; Fig. 3). Ostrander et al. (2017) indicated a shorter lag of 43 kyr between the deoxygenation of the water column and the widespread carbon burial of OAE 2 using thallium isotopes (Tl) linked to manganese oxide burial. Collectively, both studies indicate progressive deoxygenation prior to and into OAE 2. Our biomarker records, although limited for OAE 2 itself, build on these metal-isotope data by confirming that the expansion of water-column anoxia preceded the PZE during OAE 2 and adds new evidence that the expansion of water-column anoxia in the central Atlantic started as early as the MCE.

5.2 TEX$_{86}$ sea surface temperature estimates track marine anoxia during the Cenomanian

The prolonged deposition of organic black shales at Demerara Rise was likely facilitated by a combination of restricted palaeogeography that allowed nutrient trapping to maintain high primary productivity and enhanced preservation due to the lack of deep-water ventilation (Trabucho Alexandre et al., 2010). The Demerara region is proximal to the nearly closed Equatorial Atlantic Gateway (EAG) and could have acted as a "nutrient trap" due to dynamic estuarine circulation between south-west-flowing Tethyan waters and Pacific waters via the Central American Seaway (CAS; Berrocoso et al., 2010; Topper et al., 2011; Trabucho Alexandre et al., 2010). However, model simulations with a shallow-depth CAS configuration imply that marine anoxia within the Atlantic Ocean remains stable even without estuarine circulation (Laugié et al., 2021). This result indicates an addi-

tional causal mechanism for prolonged marine anoxia, which is likely associated with Cenomanian climatic conditions. Our biomarker data also indicate an important role of additional, potentially climatic, mechanisms by showing that water-column anoxia was not constant during the Cenomanian but progressively expanded upward into the water column.

Our TEX$_{86}$-derived SSTs (new data combined with the previously published data of Forster et al., 2007) show an early Cenomanian cooling period followed by an increase in SST from the mid-Cenomanian towards OAE 2. Notably, this gradual increase in SST up to 43 °C ± 3.5 °C coincided with the deoxygenation of the ocean in this region, from water-column anoxia to water-column euxinia, and ultimately photic zone euxinia as indicated by the appearance of DNH, lycopane, C_{35} hopanoid thiophene and isorenieratane respectively. These results extend the occurrence of marine water-column anoxia predating OAE 2 to the post-MCE late Cenomanian and directly links its expansion to SST, at least for this site (Fig. 3).

The Demerara region was likely bathed by warm saline intermediate water as a result of warm surface water at mid- to high latitudes that propagated via deep-water circulation (Friedrich et al., 2008). Therefore, we argue that the expansion of bottom-water anoxia and the oxygen minimum zone (based on our DNH and lycopane indices) was linked to the displacement of warm saline Demerara Bottom Water (DBW) which was overridden by south-west-flowing Tethyan waters (Berrocoso et al., 2010). This water mass displacement is evidenced by sharp transitions in neodymium isotopes, with Tethyan Waters having a heavier value, which is only recorded in shallow water (site 1260), in contrast to the lighter values at site 1258 that characterize DBW (Berrocoso et al., 2010). Crucially, the upper boundary of the warm saline DBW (Friedrich et al., 2008) likely fluctuated due to the high eustatic sea level associated with thermal expansion (Haq, 2014). Hence, it is probable that temperature-controlled ocean circulation and sea level sustained and controlled the Cenomanian black shale deposition through a combination of nutrient-rich and oxygen-poor deep-water convection, recycling of benthic phosphorus (Van Cappellen and Ingall, 1994; Mort et al., 2007), elevated nutrient inputs caused by warming-induced continental weathering (Monteiro et al., 2012; Nana Yobo et al., 2022), and high surface productivity. Collectively, these mechanisms suggest that water-column anoxia at the southern margin of the North Atlantic during OAE 2 interval but also during the Cenomanian was governed by palaeo-geographic configuration but modulated by long-term climate change such as temperature (SST). Most likely, this Cenomanian warming was global as it is also seen in the global compilation (O'Brien et al., 2017) and driven by volcanism-induced increases in CO_2 (Barclay et al., 2010).

To explore the partial pressure of atmospheric carbon dioxide (pCO$_2$) during this time, we also determined the

δ^{13}C values of the marine photoautotroph biomarker phytane (see Supplement). The δ^{13}C values of phytane are low (among the lowest of the Phanerozoic), confirming high pCO$_2$ during the Cenomanian (Supplement; Table 3). Phytane δ^{13}C values are also rather stable, but this is likely due to high pCO$_2$ where carbon isotope fractionation is saturated (e.g. Pancost et al., 2013) rather than a lack of pCO$_2$ change. Due to the lack of carbonate for most of our samples, we cannot rigorously determine carbon isotope fractionation and therefore quantify pCO$_2$. Given the SST change, it is likely that pCO$_2$ increased, but alternatively warming could have been locally amplified by an equatorward shrinkage of the Hadley circulation, causing atmospheric heat to be preserved within the equatorial region and promoting tropical warmth (Hasegawa et al., 2012). During OAE 2, phytane δ^{13}C increased dramatically, very likely indicating a pCO$_2$ decrease and a negative feedback on global warming via widespread organic carbon burial as extensively discussed elsewhere (e.g. Sinninghe Damsté et al., 2008).

Although inferred pCO$_2$ rise and SST warming appear closely linked to the expansion of anoxia during the Cenomanian, they were likely not the primary driver of long-term anoxia in the basin. The abrupt termination of OAE 2 and the associated decline in TOC content, lycopane and DNH indices and, isorenieratane abundances occurred despite elevated SSTs that persisted into the Turonian. Similarly, this persistent warming is also recorded at other sites (Robinson et al., 2019). Such continuously high SSTs appear to be linked to elevated atmospheric CO$_2$ driven by continuous volcanic outgassing (Robinson et al., 2019) that outlasted the carbon drawdown caused by widespread organic carbon burial during OAE 2.

Regardless of the mechanism, decoupling of our SST record from redox indicators confirms that temperature was not the only driver of water-column anoxia, at least at Demerara Rise after OAE 2. We suggest that the termination of anoxic conditions at Demerara Rise was related to the exhaustion of nutrients and the collapse of elevated primary productivity (Owens et al., 2016) or due to the tectonic opening of the EAG that reconfigured North Atlantic Ocean circulation such that it no longer acted as a nutrient trap (Berrocoso et al., 2010). As such, our collective Cenomanian records document a long-term increase in SST that caused Demerara Rise to cross several thresholds with respect to water-column structure, productivity, and redox conditions.

These water-column anoxia and euxinia proxies also vary dramatically throughout the Cenomanian, and future work should develop higher-resolution records that could explore whether they were modulated by short-term astronomical forcing (Nederbragt et al., 2005). For example, Laurin et al. (2016) showed that 405 kyr eccentricity modulates anoxia in the Cenomanian Mediterranean. Variations in our Demerara Rise SST and anoxia records are consistent with such pacing (e.g. maxima in eccentricity at Ce-2 and Ce-3 spanning 95 to 94 Ma), suggesting that similar orbital forcing modulated anoxia in the equatorial Atlantic. Ultimately, we propose that these observations might be linked to the nutrient status of the site, with factors like temperature-modulated upwelling and hydrology-induced weathering contributing to enhanced nutrient delivery over various timescales.

6 Conclusions

We show that Demerara Rise experienced water-column anoxia during the late Cenomanian leading up to the OAE 2 and that its expansion was driven by warming. Water-column anoxia is evidenced by the abundances of 28,30-dinorhopane and lycopane, which indicate the expansion of water-column anoxia and the oxygen minimum zone at Demerara Rise. The deoxygenated water column evolved towards more extreme sulfidic conditions during the latter part of the Cenomanian, and euxinic conditions reached the photic zone during OAE 2, as indicated by the presence of C$_{35}$ hopanoid thiophene and isorenieratane respectively. This equatorial Atlantic evolution of marine anoxia appears to be closely linked to temperature rise, only becoming decoupled after OAE 2 interval and the tectonic opening of the North Atlantic, suggesting that geography was a crucial pre-condition for the development of anoxia, albeit modulated by climatic factors.

Author contributions. MAFA, BDAN and RDP designed this study. MAFA performed the organic geochemical analyses. MAFA and VL generated the SST reconstructions using MATLAB. FS generated the bulk stable carbon isotopes. MAFA, BDAN, VL, and RDP discussed and interpreted the data. MAFA wrote the paper, with input from all authors.

References

Adam, P., Schaeffer, P., and Albrecht, P.: C40 monoaromatic lycopane derivatives as indicators of the contribution of the alga Botryococcus braunii race L to the organic matter of Messel oil shale (Eocene, Germany), Org. Geochem., 37, 584–596, https://doi.org/10.1016/j.orggeochem.2006.01.001, 2006.

Arthur, M. A., Schlanger, S. O., and Jenkyns, H. C.: The Cenomanian-Turonian Oceanic Anoxic Event, II. Palaeoceanographic controls on organic-matter production and preservation, Geol. Soc. Spec. Publ., 26, 401–420, https://doi.org/10.1144/GSL.SP.1987.026.01.25, 1987.

Arthur, M. A., Dean, W. E., and Pratt, L. M.: Geochemical and climatic effects of increased marine organic carbon burial at the Cenomanian/Turonian boundary, Nature, Nature Publishing Group, 714–717 pp., https://doi.org/10.1038/335714a0, 1988.

Barclay, R. S., McElwain, J. C., and Sageman, B. B.: Carbon sequestration activated by a volcanic CO_2 pulse during Ocean Anoxic Event 2, Nat. Geosci., 3, 205–208, https://doi.org/10.1038/ngeo757, 2010.

Batenburg, S. J., De Vleeschouwer, D., Sprovieri, M., Hilgen, F. J., Gale, A. S., Singer, B. S., Koeberl, C., Coccioni, R., Claeys, P., and Montanari, A.: Orbital control on the timing of oceanic anoxia in the Late Cretaceous, Clim. Past, 12, 1995–2009, https://doi.org/10.5194/cp-12-1995-2016, 2016.

Berrocoso, Á. J., MacLeod, K. G., Martin, E. E., Bourbon, E., Londoño, C. I., and Basak, C.: Nutrient trap for Late Cretaceous organic-rich black shales in the tropical North Atlantic, Geology, 38, 1111–1114, https://doi.org/10.1130/G31195.1, 2010.

Burdige, D. J.: Preservation of organic matter in marine sediments: Controls, mechanisms, and an imbalance in sediment organic carbon budgets?, Chem. Rev., 107, 467–485, https://doi.org/10.1021/cr050347q, 2007.

Van Cappellen, P. and Ingall, E. D.: Benthic phosphorus regeneration, net primary production, and ocean anoxia: A model of the coupled marine biogeochemical cycles of carbon and phosphorus, Paleoceanography, 9, 677–692, https://doi.org/10.1029/94PA01455, 1994.

Clarkson, M. O., Stirling, C. H., Jenkyns, H. C., Dickson, A. J., Porcelli, D., Moy, C. M., Von Strandmann, P. P. A. E., Cooke, I. R., and Lenton, T. M.: Uranium isotope evidence for two episodes of deoxygenation during Oceanic Anoxic Event 2, P. Natl. Acad. Sci. USA, 115, 2918–2923, https://doi.org/10.1073/pnas.1715278115, 2018.

Donnadieu, Y., Pucéat, E., Moiroud, M., Guillocheau, F., and Deconinck, J. F.: A better-ventilated ocean triggered by Late Cretaceous changes in continental configuration, Nat. Commun., 7, 1–12, https://doi.org/10.1038/ncomms10316, 2016.

Eldrett, J. S., Ma, C., Bergman, S. C., Lutz, B., Gregory, F. J., Dodsworth, P., Phipps, M., Hardas, P., Minisini, D., Ozkan, A., Ramezani, J., Bowring, S. A., Kamo, S. L., Ferguson, K., Macaulay, C., and Kelly, A. E.: An astronomically calibrated stratigraphy of the Cenomanian, Turonian and earliest Coniacian from the Cretaceous Western Interior Seaway, USA: Implications for global chronostratigraphy, Cretac. Res., 56, 316–344, https://doi.org/10.1016/j.cretres.2015.04.010, 2015.

Erbacher, J., Mosher, D. C., Malone, M. J., and Shipboard Scientific Party, T.: Site 1258, Proc. Ocean Drill. Program, 207 Initial Reports, 207, 1–117, https://doi.org/10.2973/odp.proc.ir.207.105.2004, 2004.

Erbacher, J., Friedrich, O., Wilson, P. A., Birch, H., and Mutterlose, J.: Stable organic carbon isotope stratigraphy across Oceanic Anoxic Event 2 of Demerara Rise, western tropical Atlantic, Geochem., Geophys. Geosyst., 6, Q06010, https://doi.org/10.1029/2004GC000850, 2005.

Forster, A., Schouten, S., Baas, M., and Sinninghe Damsté, J. S.: Mid-Cretaceous (Albian-Santonian) sea surface temperature record of the tropical Atlantic Ocean, Geology, 35, 919–922, https://doi.org/10.1130/G23874A.1, 2007.

French, K. L., Rocher, D., Zumberge, J. E., and Summons, R. E.: Assessing the distribution of sedimentary C40 carotenoids through time, Geobiology, 13, 139–151, https://doi.org/10.1111/GBI.12126, 2015.

Friedrich, O. and Erbacher, J.: Benthic foraminiferal assemblages from Demerara Rise (ODP Leg 207, western tropical Atlantic): possible evidence for a progressive opening of the Equatorial Atlantic Gateway, Cretac. Res., 27, 377–397, https://doi.org/10.1016/j.cretres.2005.07.006, 2006.

Friedrich, O., Erbacher, J., Moriya, K., Wilson, P. A., and Kuhnert, H.: Warm saline intermediate waters in the Cretaceous tropical Atlantic ocean, Nat. Geosci., 1, 453–457, https://doi.org/10.1038/ngeo217, 2008.

Friedrich, O., Erbacher, J., Wilson, P. A., Moriya, K., and Mutterlose, J.: Paleoenvironmental changes across the Mid Cenomanian Event in the tropical Atlantic Ocean (Demerara Rise, ODP Leg 207) inferred from benthic foraminiferal assemblages, Mar. Micropaleontol., 71, 28–40, https://doi.org/10.1016/j.marmicro.2009.01.002, 2009.

Frieling, J., Reichart, G.-J., Middelburg, J. J., Röhl, U., Westerhold, T., Bohaty, S. M., and Sluijs, A.: Tropical Atlantic climate and

ecosystem regime shifts during the Paleocene–Eocene Thermal Maximum, Clim. Past, 14, 39–55, https://doi.org/10.5194/cp-14-39-2018, 2018.

Haq, B. U.: Cretaceous eustasy revisited, Glob. Planet. Change, 113, 44–58, https://doi.org/10.1016/j.gloplacha.2013.12.007, 1 February, 2014.

Hasegawa, H., Tada, R., Jiang, X., Suganuma, Y., Imsamut, S., Charusiri, P., Ichinnorov, N., and Khand, Y.: Drastic shrinking of the Hadley circulation during the mid-Cretaceous Supergreenhouse, Clim. Past, 8, 1323–1337, https://doi.org/10.5194/cp-8-1323-2012, 2012.

Hedges, J. I. and Stern, J. H.: Carbon and nitrogen determinations of carbonate-containing solids, Limnol. Oceanogr., 3, https://doi.org/10.4319/lo.1984.29.3.0657, May 1984.

Hetzel, A., Brumsack, H.-J., Schnetger, B., and Böttcher, M. E.: Inorganic geochemical characterization of lithologic units recovered during ODP Leg 207 (Demerara Rise), in: Proc. ODP, Sci. Results, edited by: Mosher, D. C., Erbacher, J., and Malone, M. J., 207, College Station, TX (Ocean Drilling Program), 1–37, https://doi.org/10.2973/odp.proc.sr.207.107.2006, 2006.

Hopmans, E. C., Weijers, J. W. H., Schefuß, E., Herfort, L., Sinninghe Damsté, J. S., and Schouten, S.: A novel proxy for terrestrial organic matter in sediments based on branched and isoprenoid tetraether lipids, Earth Planet. Sci. Lett., 224, 107–116, https://doi.org/10.1016/j.epsl.2004.05.012, 2004.

Hopmans, E. C., Schouten, S., and Sinninghe Damsté, J. S.: The effect of improved chromatography on GDGT-based palaeoproxies, Org. Geochem., 93, 1–6, https://doi.org/10.1016/j.orggeochem.2015.12.006, 2016.

Hülse, D., Arndt, S., and Ridgwell, A.: Mitigation of Extreme Ocean Anoxic Event Conditions by Organic Matter Sulfurization, Paleoceanogr. Paleoclimatology, 34, 476–489, https://doi.org/10.1029/2018PA003470, 2019.

Jarvis, I., Gale, A. S., Jenkyns, H. C., and Pearce, M. A.: Secular variation in Late Cretaceous carbon isotopes: A new δ^{13}C carbonate reference curve for the Cenomanian-Campanian (99.6–70.6 Ma), Geol. Mag., 143, 561–608, https://doi.org/10.1017/S0016756806002421, 2006.

Jarvis, I., Lignum, J. S., Grcke, D. R., Jenkyns, H. C., and Pearce, M. A.: Black shale deposition, atmospheric CO_2 drawdown, and cooling during the Cenomanian-Turonian Oceanic Anoxic Event, Paleoceanography, 26, 1–17, https://doi.org/10.1029/2010PA002081, 2011.

Jenkyns, H. C.: Geochemistry of oceanic anoxic events, Geochem. Geophys. Geosyst., 11, Q03004, https://doi.org/10.1029/2009GC002788, 2010.

Joo, Y. J. and Sageman, B. B.: Cenomanian to campanian carbon isotope chemostratigraphy from the Western Interior Basin, U.S.A., J. Sediment. Res., 84, 529–542, https://doi.org/10.2110/jsr.2014.38, 2014.

Joo, Y. J., Sageman, B. B., and Hurtgen, M. T.: Data-model comparison reveals key environmental changes leading to Cenomanian-Turonian Oceanic Anoxic Event 2, https://doi.org/10.1016/j.earscirev.2020.103123, 1 April 2020.

Kim, J. H., van der Meer, J., Schouten, S., Helmke, P., Willmott, V., Sangiorgi, F., Koç, N., Hopmans, E. C., and Damsté, J. S. S.: New indices and calibrations derived from the distribution of crenarchaeal isoprenoid tetraether lipids: Implications for past sea surface temperature reconstructions, Geochim. Cosmochim.

Acta, 74, 4639–4654, https://doi.org/10.1016/j.gca.2010.05.027, 2010.

Koopmans, M. P., Köster, J., Van Kaam-Peters, H. M. E., Kenig, F., Schouten, S., Hartgers, W. A., De Leeuw, J. W., and Sinninghe Damsté, J. S.: Diagenetic and catagenetic products of isorenieratene: Molecular indicators for photic zone anoxia, Geochim. Cosmochim. Acta, 60, 4467–4496, https://doi.org/10.1016/S0016-7037(96)00238-4, 1996.

Laugié, M., Donnadieu, Y., Ladant, J. B., Bopp, L., Ethé, C., and Raisson, F.: Exploring the Impact of Cenomanian Paleogeography and Marine Gateways on Oceanic Oxygen, Paleoceanogr. Paleoclimatology, 36, e2020PA004202, https://doi.org/10.1029/2020PA004202, 2021.

Laurin, J., Meyers, S. R., Galeotti, S., and Lanci, L.: Frequency modulation reveals the phasing of orbital eccentricity during Cretaceous Oceanic Anoxic Event II and the Eocene hyperthermals, Earth Planet. Sci. Lett., 442, 143–156, https://doi.org/10.1016/j.epsl.2016.02.047, 2016.

Li, Y. X., Montañez, I. P., Liu, Z., and Ma, L.: Astronomical constraints on global carbon-cycle perturbation during Oceanic Anoxic Event 2 (OAE2), Earth Planet. Sci. Lett., 462, 35–46, https://doi.org/10.1016/j.epsl.2017.01.007, 2017.

Lüning, S., Kolonic, S., Belhadj, E. M., Belhadj, Z., Cota, L., Barić, G., and Wagner, T.: Integrated depositional model for the Cenomanian-Turonian organic-rich strata in North Africa, Earth-Sci. Rev., 64, 51–117, https://doi.org/10.1016/S0012-8252(03)00039-4, 2004.

Ma, J., French, K. L., Cui, X., Bryant, D. A., and Summons, R. E.: Carotenoid biomarkers in Namibian shelf sediments: Anoxygenic photosynthesis during sulfide eruptions in the Benguela Upwelling System, P. Natl. Acad. Sci. USA, 118, e2106040118, https://doi.org/10.1073/pnas.2106040118, 2021.

Meyers, S. R., Sageman, B. B., and Arthur, M. A.: Obliquity forcing of organic matter accumulation during Oceanic Anoxic Event 2, Paleoceanography, 27, PA3212, https://doi.org/10.1029/2012PA002286, 2012.

Moldowan, J. M., Seifert, W. K., Arnold, E., and Clardy, J.: Structure proof and significance of stereoisomeric 28,30-bisnorhopanes in petroleum and petroleum source rocks, Geochim. Cosmochim. Acta, 48, 1651–1661, https://doi.org/10.1016/0016-7037(84)90334-X, 1984.

Monteiro, F. M., Pancost, R. D., Ridgwell, A., and Donnadieu, Y.: Nutrients as the dominant control on the spread of anoxia and euxinia across the Cenomanian-Turonian oceanic anoxic event (OAE2): Model-data comparison, Paleoceanography, 27, PA4209, https://doi.org/10.1029/2012PA002351, 2012.

Mort, H. P., Adatte, T., Föllmi, K. B., Keller, G., Steinmann, P., Matera, V., Berner, Z., and Stüben, D.: Phosphorus and the roles of productivity and nutrient recycling during oceanic anoxic event 2, Geology, 35, 483–486, https://doi.org/10.1130/G23475A.1, 2007.

Naafs, B. D. A., Monteiro, F. M., Pearson, A., Higgins, M. B., Pancost, R. D., and Ridgwell, A.: Fundamentally different global marine nitrogen cycling in response to severe ocean deoxygenation, P. Natl. Acad. Sci. USA, 116, 24979–24984, https://doi.org/10.1073/pnas.1905553116, 2019.

Nana Yobo, L., Brandon, A. D., Lauckner, L. M., Eldrett, J. S., Bergman, S. C., and Minisini, D.: Enhanced continental weathering activity at the onset of the mid-Cenomanian

Event (MCE), Geochemical Perspect. Lett., 23, 17–22, https://doi.org/10.7185/geochemlet.2231, 2022.

Nederbragt, A. J., Thurow, J., and Pearce, R.: Sediment composition and cyclicity in the Mid-Cretaceous at Demerara Rise, ODP Leg 207, Proc. Ocean Drill. Progr. Sci. Results, 207, 1–31, https://doi.org/10.2973/odp.proc.sr.207.103.2007, 2005.

O'Brien, C. L., Robinson, S. A., Pancost, R. D., Sinninghe Damsté, J. S., Schouten, S., Lunt, D. J., Alsenz, H., Bornemann, A., Bottini, C., Brassell, S. C., Farnsworth, A., Forster, A., Huber, B. T., Inglis, G. N., Jenkyns, H. C., Linnert, C., Littler, K., Markwick, P., McAnena, A., Mutterlose, J., Naafs, B. D. A., Püttmann, W., Sluijs, A., van Helmond, N. A. G. M., Vellekoop, J., Wagner, T., and Wrobel, N. E.: Cretaceous sea-surface temperature evolution: Constraints from TEX86 and planktonic foraminiferal oxygen isotopes, Earth-Sci. Rev., 172, 224–247, https://doi.org/10.1016/j.earscirev.2017.07.012, 1 September 2017.

Ostrander, C. M., Owens, J. D., and Nielsen, S. G.: Constraining the rate of oceanic deoxygenation leading up to a Cretaceous Oceanic Anoxic Event (OAE-2: ∼ 94 Ma), Sci. Adv., 3, e1701020, https://doi.org/10.1126/sciadv.1701020, 2017.

Owens, J. D., Reinhard, C. T., Rohrssen, M., Love, G. D., and Lyons, T. W.: Empirical links between trace metal cycling and marine microbial ecology during a large perturbation to Earth's carbon cycle, Earth Planet. Sci. Lett., 449, 407–417, https://doi.org/10.1016/j.epsl.2016.05.046, 2016.

Pancost, R. D., Freeman, K. H., Herrmann, A. D., Patzkowsky, M. E., Ainsaar, L., and Martma, T.: Reconstructing Late Ordovician carbon cycle variations, Geochim. Cosmochim. Acta, 105, 433–454, https://doi.org/10.1016/j.gca.2012.11.033, 2013.

Peters, K. E., Walters, C. C., and Moldowan, J. M.: The Biomarker Guide, 2nd Edn., Cambridge: Cambridge University Press, https://doi.org/10.1017/cbo9781107326040, 2004.

Pogge Von Strandmann, P. A. E., Jenkyns, H. C., and Woodfine, R. G.: Lithium isotope evidence for enhanced weathering during Oceanic Anoxic Event 2, Nat. Geosci., 6, 668–672, https://doi.org/10.1038/ngeo1875, 2013.

Rattanasriampaipong, R., Zhang, Y. G., Pearson, A., Hedlund, B. P., and Zhang, S.: Archaeal lipids trace ecology and evolution of marine ammonia-oxidizing archaea, P. Natl. Acad. Sci. USA, 119, 1–10, https://doi.org/10.1073/pnas.2123193119, 2022.

Raven, M. R., Fike, D. A., Gomes, M. L., Webb, S. M., Bradley, A. S., and McClelland, H. L. O.: Organic carbon burial during OAE2 driven by changes in the locus of organic matter sulfurization, Nat. Commun., 9, 1–9, https://doi.org/10.1038/s41467-018-05943-6, 2018.

Robinson, S. A., Dickson, A. J., Pain, A., Jenkyns, H. C., O'Brien, C. L., Farnsworth, A., and Lunt, D. J.: Southern Hemisphere sea-surface temperatures during the Cenomanian-Turonian: Implications for the termination of Oceanic Anoxic Event 2, Geology, 47, 131–134, https://doi.org/10.1130/G45842.1, 2019.

Sageman, B. B., Meyers, S. R., and Arthur, M. A.: Orbital time scale and new C-isotope record for Cenomanian-Turonian boundary stratotype, Geology, 34, 125–128, https://doi.org/10.1130/G22074.1, 2006.

Scaife, J. D., Ruhl, M., Dickson, A. J., Mather, T. A., Jenkyns, H. C., Percival, L. M. E., Hesselbo, S. P., Cartwright, J., Eldrett, J. S., Bergman, S. C., and Minisini, D.: Sedimentary Mercury Enrichments as a Marker for Subma-

rine Large Igneous Province Volcanism? Evidence From the Mid-Cenomanian Event and Oceanic Anoxic Event 2 (Late Cretaceous), Geochem. Geophys. Geosyst., 18, 4253–4275, https://doi.org/10.1002/2017GC007153, 2017.

Schimmelmann, A., Qi, H., Coplen, T. B., Brand, W. A., Fong, J., Meier-Augenstein, W., Kemp, H. F., Toman, B., Ackermann, A., Assonov, S., Aerts-Bijma, A. T., Brejcha, R., Chikaraishi, Y., Darwish, T., Elsner, M., Gehre, M., Geilmann, H., Gröning, M., Hélie, J. F., Herrero-Martín, S., Meijer, H. A. J., Sauer, P. E., Sessions, A. L., and Werner, R. A.: Organic Reference Materials for Hydrogen, Carbon, and Nitrogen Stable Isotope-Ratio Measurements: Caffeines, n-Alkanes, Fatty Acid Methyl Esters, Glycines, l -Valines, Polyethylenes, and Oils, Anal. Chem., 88, 4294–4302, https://doi.org/10.1021/acs.analchem.5b04392, 2016.

Schlanger, S. and Jenkyns, H.: Cretaceous oceanic anoxic event cause an consequences, Geol. Mijnb., 55, 179–184, 1976.

Schlanger, S. O., Arthur, M. A., Jenkyns, H. C., and Scholle, P. A.: The Cenomanian-Turonian Oceanic Anoxic Event, I. Stratigraphy and distribution of organic carbon-rich beds and the marine δ13C excursion, Geol. Soc. Spec. Publ., 26, 371–399, https://doi.org/10.1144/GSL.SP.1987.026.01.24, 1987.

Schouten, S., Hopmans, E. C., Schefuß, E., and Sinninghe Damsté, J. S.: Distributional variations in marine crenarchaeotal membrane lipids: A new tool for reconstructing ancient sea water temperatures?, Earth Planet. Sci. Lett., 204, 265–274, https://doi.org/10.1016/S0012-821X(02)00979-2, 2002.

Schouten, S., Hopmans, E. C., Rosell-Melé, A., Pearson, A., Adam, P., Bauersachs, T., Bard, E., Bernasconi, S. M., Bianchi, T. S., Brocks, J. J., Carlson, L. T., Castañeda, I. S., Derenne, S., Selver, A. D., Dutta, K., Eglinton, T., Fosse, C., Galy, V., Grice, K., Hinrichs, K. U., Huang, Y., Huguet, A., Huguet, C., Hurley, S., Ingalls, A., Jia, G., Keely, B., Knappy, C., Kondo, M., Krishnan, S., Lincoln, S., Lipp, J., Mangelsdorf, K., Martínez-García, A., Ménot, G., Mets, A., Mollenhauer, G., Ohkouchi, N., Ossebaar, J., Pagani, M., Pancost, R. D., Pearson, E. J., Peterse, F., Reichart, G. J., Schaeffer, P., Schmitt, G., Schwark, L., Shah, S. R., Smith, R. W., Smittenberg, R. H., Summons, R. E., Takano, Y., Talbot, H. M., Taylor, K. W. R., Tarozo, R., Uchida, M., Van Dongen, B. E., Van Mooy, B. A. S., Wang, J., Warren, C., Weijers, J. W. H., Werne, J. P., Woltering, M., Xie, S., Yamamoto, M., Yang, H., Zhang, C. L., Zhang, Y., Zhao, M., and Damsté, J. S. S.: An interlaboratory study of TEX86 and BIT analysis of sediments, extracts, and standard mixtures, Geochem. Geophys. Geosyst., 14, 5263–5285, https://doi.org/10.1002/2013GC004904, 2013.

Schröder-Adams, C. J., Herrle, J. O., Selby, D., Quesnel, A., and Froude, G.: Influence of the High Arctic Igneous Province on the Cenomanian/Turonian boundary interval, Sverdrup Basin, High Canadian Arctic, Earth Planet. Sci. Lett., 511, 76–88, https://doi.org/10.1016/j.epsl.2019.01.023, 2019.

Scotese, C. R.: An atlas of phanerozoic paleogeographic maps: The seas come in and the seas go out, Annu. Rev. Earth Planet. Sci., 49, 679–728, https://doi.org/10.1146/annurev-earth-081320-064052, 30 May 2021.

Sinninghe Damsté, J. S. and Köster, J.: A euxinic southern North Atlantic Ocean during the Cenomanian/Turonian oceanic anoxic event, Earth Planet. Sci. Lett., 158, 165–173, https://doi.org/10.1016/S0012-821X(98)00052-1, 1998.

Sinninghe Damsté, J. S., Kohnen, M. E. L., and De Leeuw, J. W.: Thiophenic biomarkers for palaeoenvironmental assessment and molecular stratigraphy, Nature, 345, 609–611, https://doi.org/10.1038/345609a0, 1990.

Sinninghe Damsté, J. S., Van Duin, A. C. T., Hollander, D., Kohnen, M. E. L., and De Leeuw, J. W.: Early diagenesis of bacteriohopanepolyol derivatives: Formation of fossil homohopanoids, Geochim. Cosmochim. Acta, 59, 5141–5157, https://doi.org/10.1016/0016-7037(95)00338-X, 1995.

Sinninghe Damsté, J. S., Schouten, S., and Van Duin, A. C. T.: Isorenieratene derivatives in sediments: Possible controls on their distribution, Geochim. Cosmochim. Acta, 65, 1557–1571, https://doi.org/10.1016/S0016-7037(01)00549-X, 2001.

Sinninghe Damsté, J. S., Kuypers, M. M. M., Schouten, S., Schulte, S., and Rullkötter, J.: The lycopane/C31 n-alkane ratio as a proxy to assess palaeoxicity during sediment deposition, Earth Planet. Sci. Lett., 209, 215–226, https://doi.org/10.1016/S0012-821X(03)00066-9, 2003.

Sinninghe Damsté, J. S., Kuypers, M. M. M., Pancost, R. D., and Schouten, S.: The carbon isotopic response of algae, (cyano)bacteria, archaea and higher plants to the late Cenomanian perturbation of the global carbon cycle: Insights from biomarkers in black shales from the Cape Verde Basin (DSDP Site 367), Org. Geochem., 39, 1703–1718, https://doi.org/10.1016/j.orggeochem.2008.01.012, 2008.

Sinninghe Damsté, J. S., van Bentum, E. C., Reichart, G. J., Pross, J., and Schouten, S.: A CO_2 decrease-driven cooling and increased latitudinal temperature gradient during the mid-Cretaceous Oceanic Anoxic Event 2, Earth Planet. Sci. Lett., 293, 97–103, https://doi.org/10.1016/j.epsl.2010.02.027, 2010.

Sinninghe Damsté, J. S., Ossebaar, J., Schouten, S., and Verschuren, D.: Distribution of tetraether lipids in the 25-ka sedimentary record of Lake Challa: Extracting reliable TEX 86 and MBT/CBT palaeotemperatures from an equatorial African lake, Quaternary Sci. Rev., 50, 43–54, https://doi.org/10.1016/j.quascirev.2012.07.001, 2012.

Sinninghe Damsté, J. S., Schouten, S., and Volkman, J. K.: C27-C30 neohop-13(18)-enes and their saturated and aromatic derivatives in sediments: Indicators for diagenesis and water column stratification, Geochim. Cosmochim. Acta, 133, 402–421, https://doi.org/10.1016/j.gca.2014.03.008, 2014.

Słowakiewicz, M., Tucker, M. E., Perri, E., and Pancost, R. D.: Nearshore euxinia in the photic zone of an ancient sea, Palaeogeogr. Palaeoclimatol. Palaeoecol., 426, 242–259, https://doi.org/10.1016/j.palaeo.2015.03.022, 2015.

Snow, L. J., Duncan, R. A., and Bralower, T. J.: Trace element abundances in the Rock Canyon Anticline, Pueblo, Colorado, marine sedimentary section and their relationship to Caribbean plateau construction and ocean anoxic event 2, Paleoceanography, 20, 1–14, https://doi.org/10.1029/2004PA001093, 2005.

Takashima, R., Nishi, H., Yamanaka, T., Hayashi, K., Waseda, A., Obuse, A., Tomosugi, T., Deguchi, N., and Mochizuki, S.: High-resolution terrestrial carbon isotope and planktic foraminiferal records of the Upper Cenomanian to the Lower Campanian in the Northwest Pacific, Earth Planet. Sci. Lett., 289, 570–582, https://doi.org/10.1016/j.epsl.2009.11.058, 2010.

Taylor, K. W. R., Huber, M., Hollis, C. J., Hernandez-Sanchez, M. T., and Pancost, R. D.: Re-evaluating modern and Palaeogene GDGT distributions: Implications for SST reconstructions, https://doi.org/10.1016/j.gloplacha.2013.06.011, 1 September 2013.

Tierney, J. E. and Tingley, M. P.: A Bayesian, spatially-varying calibration model for the TEX86 proxy, Geochim. Cosmochim. Acta, 127, 83–106, https://doi.org/10.1016/j.gca.2013.11.026, 2014.

Topper, R. P. M., Trabucho Alexandre, J., Tuenter, E., and Meijer, P. Th.: A regional ocean circulation model for the mid-Cretaceous North Atlantic Basin: implications for black shale formation, Clim. Past, 7, 277–297, https://doi.org/10.5194/cp-7-277-2011, 2011.

Trabucho Alexandre, J., Tuenter, E., Henstra, G. A., Van Der Zwan, K. J., Van De Wal, R. S. W., Dijkstra, H. A., and De Boer, P. L.: The mid-Cretaceous North Atlantic nutrient trap: Black shales and OAEs, Paleoceanography, 25, PA4201, https://doi.org/10.1029/2010PA001925, 2010.

Valisolalao, J., Perakis, N., Chappe, B., and Albrecht, P.: A novel sulfur containing C35 hopanoid in sediments, Tetrahedron Lett., 25, 1183–1186, https://doi.org/10.1016/S0040-4039(01)91555-2, 1984.

van Bentum, E. C., Hetzel, A., Brumsack, H. J., Forster, A., Reichart, G. J., and Sinninghe Damsté, J. S.: Reconstruction of water column anoxia in the equatorial Atlantic during the Cenomanian-Turonian oceanic anoxic event using biomarker and trace metal proxies, Palaeogeogr. Palaeoclimatol. Palaeoecol., 280, 489–498, https://doi.org/10.1016/j.palaeo.2009.07.003, 2009.

Voigt, S., Erbacher, J., Mutterlose, J., Weiss, W., Westerhold, T., Wiese, F., Wilmsen, M., and Wonik, T.: The Cenomanian – Turonian of the Wunstorf section – (North Germany): Global stratigraphic reference section and new orbital time scale for Oceanic Anoxic Event 2, Newsletters Stratigr., 43, 65–89, https://doi.org/10.1127/0078-0421/2008/0043-0065, 2008.

Weijers, J. W. H., Schouten, S., Spaargaren, O. C., and Sinninghe Damsté, J. S.: Occurrence and distribution of tetraether membrane lipids in soils: Implications for the use of the TEX86 proxy and the BIT index, Org. Geochem., 37, 1680–1693, https://doi.org/10.1016/j.orggeochem.2006.07.018, 2006.

Werne, J. P., Hollander, D. J., Lyons, T. W., and Sinninghe Damsté, J. S.: Organic sulfur biogeochemistry: Recent advances and future research directions, Spec. Pap. Geol. Soc. Am., 379, 135–150, https://doi.org/10.1130/0-8137-2379-5.135, 2004.

Zhang, Y. G., Zhang, C. L., Liu, X. L., Li, L., Hinrichs, K. U., and Noakes, J. E.: Methane Index: A tetraether archaeal lipid biomarker indicator for detecting the instability of marine gas hydrates, Earth Planet. Sci. Lett., 307, 525–534, https://doi.org/10.1016/j.epsl.2011.05.031, 2011.